J Intell Robot Syst (2016) 82:3–19
DOI 10.1007/s10846-015-0250-y

Virtual Impedance Control for Safe Human-Robot Interaction

Sheng-Yen Lo · Ching-An Cheng · Han-Pang Huang

Received: 17 February 2015 / Accepted: 25 June 2015 / Published online: 23 July 2015

Abstract Collision avoidance is essential for safe robot manipulation. Especially with humans around, robots should work only when safety can be robustly guaranteed. In this paper, we propose using virtual impedance control for reactive, smooth, and consistent collision avoidance that interferes minimally with the original task. The virtual impedance control operates in the risk space, a vector space describing the possibilities of all forthcoming collisions, and is designed to elude all risks in a consistent response in order to create assuring human-robot interaction experiences. The proposed scheme intrinsically handles kinematic singularity and the activation of avoidance using a boundary layer defined on the spectrum of Jacobian. In cooperation with the original controller, the proposed avoidance scheme provides a proof of convergence if the original controller is stable with and without projection. In simulations and experiments, we verified the characteristics of the proposed control scheme and integrated the system with Microsoft Kinect to monitor the workspace for real-time collision detection and avoidance. The results show that the proposed approach is suitable for robot operation with humans nearby.

Keywords Safe human-robot interaction · Collision avoidance · Risk space · Virtual impedance control

1 Introduction

The safety issue is particularly stressed when robots are working in close distance to humans in industrial [1–6] and domestic applications [7–9]. However, in most cases where robots' are programmed to achieve some predefined tasks, only performance indexes such as tracking error are concerned. Therefore, an additional reactive collision avoidance control is necessary for preventing potential injuries caused by physical contacts unexpected in path planning stage. Classical path planning and obstacle avoiding schemes [10], such as rapidly-exploring random tree, may be too slow to react because of the necessary global surrounding information. By contrast, reactive controls [11–16] use only local information from proximity sensors or computer vision to control the robot. On the basis of potential field [17], most approaches [12, 14, 15, 18–24] guide the robot through the environment by setting proper attractive and repulsive potentials. The forces, defined as the sum of the negative gradients

Electronic supplementary material The online version of this article (doi:10.1007/s10846-015-0250-y) contains supplementary material, which is available to authorized users.

S.-Y. Lo · C.-A. Cheng · H.-P. Huang (✉)
Department of Mechanical Engineering, National Taiwan University, Taipei, Taiwan, Republic of China
e-mail: hanpang@ntu.edu.tw

of the potentials, form a vector field and drive the robot to achieve the task while preventing collisions. As a consequence, these reactive control schemes can respond to the environment rapidly and smoothly. In [15, 20], the distances between the robot and the obstacles were computed in the proposed depth space in lieu of projecting the depth data into the configuration space. The computed distances were then employed in a potential field that allowed the robot to avoid collisions with all obstacles including humans. In [12, 14, 19, 25], with a geometrical model consisting of spherically extended convex hulls placed around the body links, the potential colliding link pairs were identified to generate repulsive forces that could maneuver the robot away from the self-collision case.

However, such an avoidance approach may fail to generalize to escape from multiple collisions, because the degrees of freedom (DOF) of the robot are finite. To address this dilemma, the literatures majorly fall into two categories according to the use of projection matrix. Without projection matrix, the first group sums the repulsive forces generated from different obstacles. In [24], the repulsive forces on the risky points were transmitted to some predefined control points to handle multiple collisions. In [14, 19, 22, 26, 27], to unify both virtual and physical forces, all repulsive forces were mapped by the corresponding Jacobian matrices and summed in joint space. Similarly, in [28], the contributions of potentials for collision avoidance, joint limit avoidance, and manipulation, were summed up to control the robot. The approach of summation is intuitive and simple, yet some underlying problems exist. Among them, the most serious one is where the equilibrium point lies. Although the system can be stabilized by introducing proper damping terms to regulate velocity, the equilibrium point cannot always be guaranteed to be collision-free.

On the contrary, null-space projection can be used to isolate the original task from collision avoidance. In [18], the original task was placed in the first priority and the collision avoidance only operated in the null-space of the original task, which is appealing for highly redundant robots. [29] designed a collision avoidance scheme in the null space of the original task, preventing the collision of the point closest with the obstacle. However, these approaches do not confront the question whether the null space of the original task can always be large enough for successful avoidance. To robustly enforce the priority of collision avoidance, [16] operated the original task only in the null space of self-collision avoidance control and defined a vector-valued potential for multiple collision points. However, due to the asymptotical nature of the design, the robot may be trapped in the potential fields.

In general, reactive control does not necessarily guarantee safety. Potentially a multi-priority problem, the safety requirement means that the collision avoidance should be placed in the top priority: the potential field should compensate for the dynamics of the point at risk, so that the chosen point can avoid the obstacle regardless of the predefined trajectory or control scheme. To this end, the original control scheme should operate in the null space of Jacobian related to the collision avoidance. This *avoidance-first* concept distinguishes itself from the *task-first* approach that uses the null space of the original task (e.g. the tracking of end-effector) for collision avoidance. In [18, 29], the task-first approach was proposed on the premise that the robot has sufficient redundancy in the null space of the primary task. Though this assumption might be true in some cases, it does not cover the scenario where the frame of the primary task directly confronts the obstacle. Alternatively, treating the collision avoidance first can deal with general situations and, similarly, does not affect the original task if any admissible solution exists. The original task will be interrupted only if there is no feasible configuration without collision.

Once the physical safety is provided, another important issue rising in human-robot interaction is the perceptional safety. In collision avoidance, this requires robots to respond in a predictable, therefore, consistent manner. One solution is to design a consistent collision dynamics on a single point and transfer the repulsive forces of other collision points to that point. In [17], when multiple potential collision points were presented, the forces originally exerted on different points were transferred to the end-effector, whose dynamics followed a unit mass model. Therefore, the collision dynamics in such transmission scheme is consistent at least in terms of the end effector, though the success of the avoidance of the whole body is uncertain. Another solution is to continuously switch between different collision points. Because only one point is selected at a time, the collision dynamics can be consistent at least in a short interval. But due to the switching, chattering may occur if multiple collision

points present with similar risks or other uncertainties, such as the discretization of control and detection.

In this paper, we propose using virtual impedance control in the risk space to design a collision avoidance scheme that is both physically and perceptionally safe. The risk space is a vector space that represents the possibilities of potential collision points. When the robot's distance to any obstacle is below a predefined threshold, the collision avoidance scheme activates and the robot dynamics is partitioned into two parts: the risk dynamics and the projected original dynamics. In the risk space, the virtual impedance control regulates the dynamics with the chosen damping ratio and bandwidth and forces the system away from the obstacles, while the original dynamics operates in the null space of the risk functions' Jacobian to accomplish the assigned task.

The proposed scheme naturally generalizes to multiple collision points and uniformly solves the singularity, the trapping, and the switching problems. We design a boundary layer defined on the spectrum of the Jacobian matrix to indicate the region where the collision avoidance just activates or the Jacobian of collision avoidance is close to singular. As the system travels into the boundary layer, the projection matrices continuously transit into weighting matrices to balance the repulsive forces and the original dynamics. Partitioning the joint space with respect to the boundary layer, we prove that the proposed virtual impedance control asymptotically converges to the attraction region of the original dynamics or to a bounded region in the boundary layer. Therefore, the proposed scheme is appealing in the sense that it exhibits only necessary distraction. In addition, because the controller works in the acceleration domain, the velocity profile of the proposed scheme is intrinsically continuous.

In the rest of this paper, we introduce the concept of risk space in Section 2, and present the proposed law in Section 3. Then we validate the proposed scheme in simulations and experiments with the 6-DOF NTU robot arm and Microsoft Kinect^{TM} in Section 4. Finally, a short conclusion is drawn in Section 5.

2 Risk Space

To model the robot, we assume that its geometry can be contained in the union of a set of fully-connected convex bodies indexed by Denavit-Hartenberg notation, as depicted in Fig. 1, where link i is connected by joint i and joint $i+1$ and frame i is assigned to joint $i+1$, with link length a_i, link twist α_i, link offset d_i, and the joint angle θ_i. The indexes of the joints from the base to the end-effector are arranged in ascending order. For links i with non-zero link length a_i or link offset d_i, its body $\mathcal{L}_i$ is modelled as the union of n_i elementary convex sets $\mathcal{L}_{i,k}$, which can be arbitrarily chosen (e.g. spherically extended line segment, rectangular, or cylinder) according to the application as long as their union

$$\mathcal{L}_i = \bigcup_{k=1}^{n_i} \mathcal{L}_{i,k} \tag{1}$$

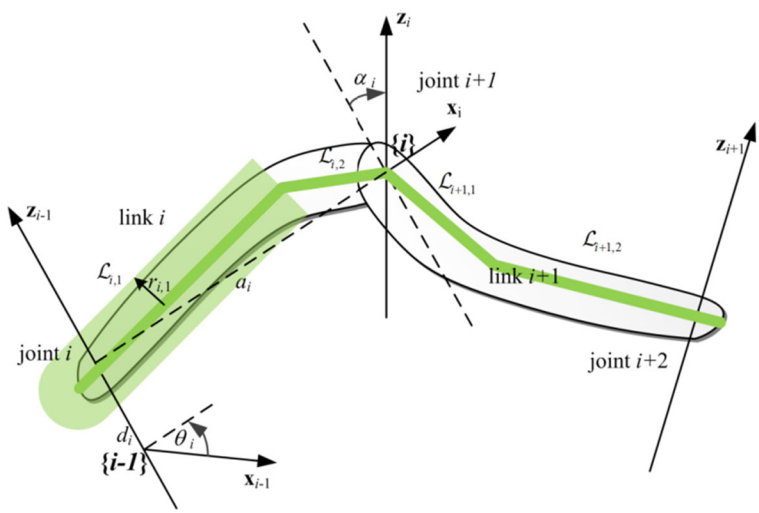

Fig. 1 The geometric model of the robotic manipulator

covers the geometry of link $i$and does not interfere with that of any non-adjacent link. As for the environment, similar models are used to approximate the geometry. Though $\mathcal{L}_i$ is not necessarily convex, it is composed by a finite set of convex bodies. Therefore, based on this description, the body-to-body collision can be efficiently prevented by computing the shortest distance between the two convex bodies.

The concept of risk space is to introduce the risk function to govern the response to potential collisions, so that different types of collisions can be avoided in a unified framework. With each entry ranging from 0 to 1, a risk function is vector-valued function representing the possibility of forthcoming collisions. An entry is 0 when a potential collision can be neglected and 1 when that collision occurs physically. In this paper, if the risk function is non-zero, the collision avoidance activates in attempt to confine the growth of the risk function.

To describe the risk space, we first enumerate all possible collisions. Suppose the number of convex bodies used to model the robot and the environment is finite. The possible collisions can be listed by a finite set

$$\mathcal{C} = \{(i, j)|i, j \in \mathbb{N}_L\} = \mathcal{C}_C \cup \mathcal{C}_J \tag{2}$$

where $\mathcal{C}_C$ is the set of collision pairs in Cartesian space, $\mathcal{C}_J$ is the set of collision pairs due to joint limit, L is the number of all the convex bodies used in modeling, and $\mathbb{N}_L := \{1, ..., L\}$. Let $q \in \mathbb{R}^n$ be the joint angle of an n-DOF robot. In this paper, we choose the risk function $r_+ \in \mathbb{R}^m$ in the form

$$r_+ = \phi(r(q)) \tag{3}$$

where m is the number of activated risks defined by $r(q)$ in Eq. 5. The transformation function $\phi : [0, 1]^m \rightarrow [0, 1]^m$ is a monotonically increasing second-order differentiable function defined for each entry of $r(q)$ satisfying

$$\begin{aligned} &\phi(0) = 0, \quad \phi(1) = 1, \quad \partial\phi,\ \partial^2\phi < \infty, \\ &\text{and} \sup_{r_+ \in [0,\delta]} \partial\phi < \varepsilon, \end{aligned} \tag{4}$$

and $\delta,\ \varepsilon > 0$ are small numbers; the ith entry $r_i(q)$ of $r(q) : \mathbb{R}^n \rightarrow [0, 1]^m$ is defined as follows: for the ith potential collision $\mathcal{P}_i$

$$r_i(q) = \frac{\bar{d}_i - d_i(q)}{\bar{d}_i}, \text{ if } \bar{d}_i \geq d_i(q) \tag{5}$$

where $\bar{d}_i$ is the size of the buffer zone, $d_i(q)$ is the shortest distance between the pair of links in the Cartesian space or the distance to the joint limit defined in the joint space. The constant $\bar{d}_i$ is chosen manually to ensure the robustness of the collision while not limiting too much workspace. In the case where the joint limit is two-sided, the pair of links is duplicated in $\mathcal{C}$ so that $d_i(q)$ in Eq. 5 becomes well defined.

Given finite pairs of collisions, the *risk space* is defined as the image of the risk function r_+ in R^m. In the risk space, r_+ is second-order differentiable with respect to q. Therefore, the velocity $\dot{r}_+$ and the acceleration $\ddot{r}_+$ exist and can be computed as

$$\dot{r}_+ = J\dot{q} \tag{6}$$

$$\ddot{r}_+ = J\ddot{q} + \dot{J}\dot{q} \tag{7}$$

where $J = J_\phi J_r$, $J_\phi = \partial\phi/\partial r$ and $J_r = \partial r/\partial q$.

To control the second-order risk space dynamics, J and $\dot{J}$ need to be known. The Jacobian matrix J defines the variation between the joint space and the risk function and can be computed by the product of J_ϕ and J_r. Because $J_\phi = \partial\phi/\partial r$ and is diagonal, J_ϕ can have an analytical form given that ϕ is user-defined. For J_r, by Eq. 5, the ith row of J_r is

$$-\bar{d}_i^{-1}\hat{d}_i^T(j_2 - j_1) \tag{8}$$

if $\mathcal{P}_i \in \mathcal{C}_C$, where $d_i = x_2 - x_1$, $\hat{d}_i = d_i/\|d_i\|$, $x_1, x_2 \in \mathbb{R}^3$ are the two vertices of the line segment of the shortest distance in $\mathcal{P}_i$, and $j_1, j_2 \in \mathbb{R}^{3\times n}$ are the Jacobian matrices of the linear velocity of points x_1 and x_2, respectively. Otherwise, if $\mathcal{P}_i \in \mathcal{C}_J$, then the ith row of J_r can be computed directly as

$$-\bar{d}_i^{-1}\frac{\partial d_i(q)}{\partial q} \tag{9}$$

which concerns only the sign of the definition of $d_i(q)$. On the other hand, $\dot{J} = \dot{J}_\phi J_r + J_\phi \dot{J}_r$. $\dot{J}_\phi$ is diagonal and its ith diagonal element is given by

$$\frac{\partial^2\phi}{\partial^2 r_i}\dot{r}_i, \tag{10}$$

which is available since $\dot{r} = J_r\dot{q}$. The ith row of $\dot{J}_r$ can be computed as

$$\begin{aligned} -\bar{d}_i^{-1}\Bigg[&\|d_i\|^{-1}\dot{q}^T(j_2 - j_1)^T\left(I - \hat{d}_i\hat{d}_i^T\right)(j_2 - j_1) \\ &+\hat{d}_i^T\frac{d}{dt}(j_2 - j_1)\Bigg] \end{aligned} \tag{11}$$

if $\mathcal{P}_i \in \mathcal{C}_J$; otherwise, it is a zero vector. Therefore, using Eqs. 6–11, all the information of the risk space dynamics up to second-order is available.

By defining the risk space, the conundrum of maintaining consistency with multiple collision points can be addressed in a unified framework. Because the risk space includes all possible collisions, we can focus on the dynamics in the risk space alone to determine the success of the collision avoidance. For consistency, we maintain the dynamics in the risk space instead of the Cartesian space or the joint space, so the dynamic behavior of the collision avoidance follows a consistent manner regardless of the number of collisions and the configuration of the robot. Additionally, because the risk function is second-order differentiable, the dynamic behavior in the risk space can be controlled as impedance control, so that the overall system can both be stable and achieve the desired response.

3 Virtual Impedance Control in the Risk Space

In the following, we consider the kinematic feedback control problem. We assume that the robot is originally stabilized with a feedback control law $\ddot{q}_o(q, \dot{q})$, which is realized as desired joint acceleration $\ddot{q}_d = \ddot{q}_o(\dot{q}, q)$. In implementation, $\ddot{q}_d$ can be a stable path generation law for a position-controlled robot, or used in the torqued-controlled robot,

$$M(q)\ddot{q} + F(q, \dot{q}) = \tau, \tag{12}$$

for example with inverse dynamics feedback, as

$$\tau = M(q)^{-1}(\ddot{q}_d + G(\dot{q}_d - \dot{q})) + F(q, \dot{q}), \tag{13}$$

where $M(q)$ denotes the inertia matrix and $F(q, \dot{q})$ denotes the Coriolis/centrifugal and gravity forces, τ is the motor torque, and $G > 0$ is the feedback gain. In the following, we consider the redesign of $\ddot{q}_d$ to avoid collision while attempting to follow the original dynamics. Instead of using Eq. 13, a direct redesign of τ can also be derived, which is similar to the following approach but using the dynamics-consistent projection [30]. Therefore, we omit it here and focus on the design of $\ddot{q}_d$ here for the space and clarity in expressing the idea.

The overall control scheme is divided into two parts: collision detection and collision avoidance. In the first stage, the value of the risk function, which represents the possibility of collisions, is continuously updated based on the closest distance between two convex bodies in the Cartesian space or the distance to the joint limit. If the risk function is non-zero, then the collision avoidance control activates. To prevent the collision regardless of scenarios, the proposed control scheme first cancels the portion of $\ddot{q}_0$ which is related to the upcoming collisions, and then adds another compensating term into $\ddot{q}_d$ such that the forthcoming collisions can be avoided smoothly.

The aims of the proposed control are that the collision avoidance is placed in the highest priority so that the original control law has no effect on the subspace that concerns the collision whenever the risk function is non-zero, and that the avoiding motion is smooth instead of stopping abruptly for better user-interaction experience. Therefore, when the collision avoidance is activated, on the subspace related to collision the system's behavior is controlled in the risk space, so that the dynamics of the collision avoidance is independent of the configuration and the types of collisions; at the same time, $\ddot{q}_0$ is maintained on the complementary space to continue the assigned task. In addition, to eliminate the inherent switching due to projection, a transition region called the *boundary layer* is designed, in which the influence of $\ddot{q}_o$ is gradually decreased and replaced by the collision avoidance control.

3.1 Virtual Impedance Control and the Boundary Layer

The control law is formulated as

$$\ddot{q}_d = \bar{P}\ddot{q}_r + \bar{N}\ddot{q}_o \tag{14}$$

where $\ddot{q}_r$ is the acceleration to achieve the desired risk space dynamics, and $\bar{P}$, $\bar{N}$ are two positive semi-definite matrices such that $\bar{P} + \bar{N} = I$, which are similar to the concept of projection and will be defined later. To control the risk dynamics, $\ddot{q}_r$ is designed with the control-Lyapunov function:

$$\mathcal{V}_R(q, \dot{q}) = \frac{k_r}{2} r_+^T r_+ + \frac{1}{2}\dot{r}_+^T \dot{r}_+ \tag{15}$$

where $k_r > 0$ is the scalar parameter controlling the bandwidth of collision avoidance motion. Because Eq. 15 is positive definite in $(r_+, \dot{r}_+)$, all the risks converge to zero if Eq. 15 converges to zero. To attain the objective, the virtual impedance control

$$\ddot{r}_+ = -b_r\dot{r}_+ - k_r r_+ \tag{16}$$

is designed with damping $b_r > 0$ to ensure that the time derivative of Eq. 15 is negative semi-definite, i.e.

$$\dot{\mathcal{V}}_R = k_r r_+^T \dot{r}_+ + \dot{r}_+^T \ddot{r}_+ = -b_r \|\dot{r}_+\|^2, \tag{17}$$

To realize Eq. 17, it is sufficient to find $\ddot{q}$ such that

$$J\ddot{q} = -b_r \dot{r}_+ - k_r r_+ - \dot{J}\dot{q}. \tag{18}$$

If Eq. 18 is satisfied, the system will converge to a positively invariant set where $\|\dot{r}_+\| = 0$ and $\|r_+\| = 0$, independent of the configuration of the robot. However, Eq. 18 does not hold in general due to the limited DOF. Let $k := rank(J)$. In particular, $k < m$ may occur even if $m < n$, because the position and the type of forthcoming obstacle is unknown beforehand. In addition, for $k = m$, the smallest non-zero singular value of J may be too small for Eq. 18 to realize.

To approximate the solution, we adopt the controller in Eq. 14 and set

$$\ddot{q}_r = -V\Sigma^{-1}U^T(k_r r_+ + \dot{J}\dot{q}) - b_r\dot{q} \tag{19}$$

and

$$\bar{P} = V\Psi V^T, \tag{20}$$

where $J = U\Sigma V^T$ is the singular value decomposition (SVD) of the Jacobian matrix with the basis $U \in \mathrm{R}^{m\times k}$, $V \in \mathrm{R}^{n\times k}$ of the non-zero singular values $\Sigma \in \mathrm{R}^{k\times k}$. The matrix $\Psi \in \mathrm{R}^{k\times k}$ is a diagonal matrix defined as

$$\Psi_{ii} = \begin{cases} 1 & \sigma_{thre} \le \sigma_i \\ \psi(\sigma_i) & 0 \le \sigma_i < \sigma_{thre} \end{cases}, \tag{21}$$

where $\psi(\sigma_i)$ is a monotonically increasing continuous function satisfying $\psi(0) = 0$ and $\psi(\sigma_{thre}) = 1$, and $\sigma_{thre} > 0$ is the threshold. Therefore, in implementation, the overall control law gives

$$\begin{aligned} \ddot{q}_d &= \bar{P}\ddot{q}_r + \bar{N}\ddot{q}_o \\ &= V\Psi V^T(-V\Sigma^{-1}U^T(k_r r_+ + \dot{J}\dot{q}) - b_r\dot{q}) \\ &\quad +(I - V\Psi V^T)\ddot{q}_o \\ &= \ddot{q}_o - V[(\Psi\Sigma^{-1})U^T(k_r r_+ + \dot{J}\dot{q}) \\ &\quad +\Psi V^T(\ddot{q}_o + b_r\dot{q})] \end{aligned} \tag{22}$$

In the region where $\sigma_i \ge \sigma_{thre}$, this control is essentially a multi-priority control where the secondary task operates in the null space of the primary task, i.e.

$$\ddot{q}_d = P\ddot{q}_r + N\ddot{q}_o, \tag{23}$$

where $\bar{P} = P := VV^T$ and $\bar{N} = N := I - P$. $N\ddot{q}_0$ projects the original dynamics into the null space of the active Jacobian matrix J, so the original dynamics will impose no effect on the risk dynamics once the collision avoidance activates. The term $P\ddot{q}_r$ controls the risk dynamics, so the risk space dynamics is consistent in the controllable subspace (i.e. the column space of the active Jacobian matrix J). Therefore, regardless of the number of the active potential collision points, the dynamics of the risk function r_+ follows a projected second-order linear system,

$$UU^T(\ddot{r}_+ + b_r\dot{r}_+ + k_r r_+) = 0, \tag{24}$$

which is characterized by the stiffness k_r and the damping b_r to realize specified bandwidth and damping ratio. Because Eq. 24 is linear, though nonlinear in terms of r, the damping ratio in can prevent the undesirable effects, such as the overshooting.

In the vicinity of singularity, Ψ_{ii} acts a spectral filter [31] such that$\Psi\Sigma^{-1} < \infty$ and therefore $P\ddot{q}_r$ is bounded. In this *boundary layer*$\{q \in \mathbb{R}^n | \exists\sigma_i < \sigma_{thre}\}$ the control law Eq. 14 uses Ψ to continuously weight $\ddot{q}_o$ and $\ddot{q}_r$ according to the size of σ_i. Because $J = J_\phi J_r$ is the product of the Jacobian of risk function and the Jacobian of kinematics, and $\sup_{r_+\in[0,\delta]} \partial\phi < \varepsilon$ is required in Eq. 5, the boundary layer contains the region of the boundary of the collision avoidance scheme (i.e.$r_+$is close to zero) as well as the region where J_r is nearly kinematically singular that physically unrealizable acceleration is needed to generate certain motions. Therefore, by defining Ψ on the spectral of J and using Eq. 22, the problem of kinematic singularity and activation of collision avoidance are resolved; the collision avoidance in these two cases does not require $\ddot{q}_o$ to be completely canceled.

On the boundary where certain elements of r_+ is close to zero, $\bar{N}\ddot{q}_o$ could act as a force to help the robot escape from the potential field in finite time. Otherwise, without the boundary layer, if $b_r \ge 2\sqrt{k_r}$ (i.e. damping ratio is larger than unity) is adopted, converges to zero as $t \to \infty$. Therefore, the robot will be trapped in the potential for collision avoidance. On the other hand, at the singularity of kinematics, though $\|r_+\|$ may be nonzero and $\ddot{q}_o$ may contribute that $\dot{r}_+^T J\ddot{q}_o > 0$, the inclusion of $\ddot{q}_o$ through $\bar{N}\ddot{q}_o$ does not pose serious threat, if σ_{thre} is small enough. Although $\|\bar{N}\ddot{q}_o\|$ increases as $\sigma_i \to 0$, $\|J\bar{N}\ddot{q}_o\|$ converges to zero because $\lim_{\sigma_i\to 0}(1 - \psi(\sigma_i))\sigma_i = 0$. Therefore, the contribution from $\ddot{q}_o$ to the increase of $\|r_+\|$ is not significant.

The idea of $\bar{P}$ is similar to the approaches using damped-least square and spectral filter, which redefine pseudo-inverse in the kinematic control near singularity, but it is based on the concept of projection matrix. In fact, using the damped pseudo-inverse $J^T(JJ^T + \varsigma^2 I)^{-1}$ effectively yields $\Psi = (\varsigma^2 I + \Sigma^2)^{-1}\Sigma^2$ with $\sigma_{thre} = \infty$ and $\varsigma > 0$; the spectral filter can also be realized by choosing proper Ψ and σ_{thre}, which satisfy the definition in Eq. 21. On the other hand, $\bar{P}$ is aimed to eliminate the chattering effect due to the discontinuity inherited from projection. In Eq. 14, if $\bar{P} = P$, then $\Psi = sgn(\Sigma > 0)$, which is discontinuous at $\Sigma = 0$ where the dimension of VV^T changes, introducing infinite fast switch near the singularity. Therefore, modifying the definition of Ψ into a continuous function can attenuate the switching.

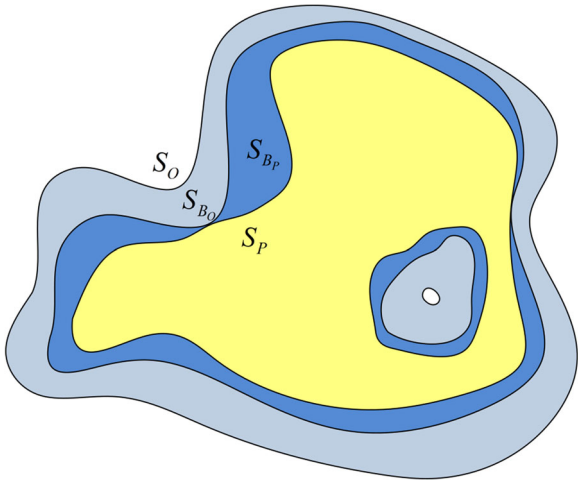

Fig. 2 The illustration of the partitions in joint space

3.2 Stability Analysis

Assume that the environment is stationary and that the original dynamics is asymptotically stable without projection and stable with projection. We first partition the joint space into four parts according to the boundary layer and singularity:

$$\begin{aligned} S_P &:= \{q \in \mathrm{R}^n | \Psi = I, k \neq 0\} \\ S_{B_P} &:= \{q \in \mathrm{R}^n | \Psi \neq I, k \neq 0\} \backslash S_{B_O} \\ S_{B_O} &:= \{q \in \mathrm{R}^n | \Psi < I, k \neq 0\} \\ S_O &:= \{q \in \mathrm{R}^n | k = 0\} \end{aligned} \tag{25}$$

S_P denotes the joint space in which the collision avoidance activates and far from singularity and the boundary;

$$S_B := S_{B_O} \cup S_{B_P} \tag{26}$$

denotes the boundary layer; S_O denotes the joint space in which the collision avoidance is inactive. By definition,

$$\begin{gathered} S_P \cap S_B = \emptyset,\ S_B \cap S_O = \emptyset,\ \text{and } S_P \cap S_O = \emptyset \\ S_P \cup S_B \cup S_O = \mathrm{R}^n \end{gathered} \tag{27}$$

Further, assume ϕ is chosen such that $\sup_{r_+ \in [0,\delta]} \partial\phi$ is small enough in respect with σ_{thre}. Then these sets form a relationship, as illustrated in Fig. 2, satisfying

$$\begin{aligned} &S_P \text{ is only connected with } S_{B_P} \\ &S_{B_P} \text{ is only connected with } S_P \text{ and } S_{B_O} \\ &S_{B_O} \text{ is only connected with } S_{B_O} \text{ and } S_O \\ &S_O \text{ is only connected with } S_{B_O} \end{aligned} \tag{28}$$

That is, these sets form a non-cyclic chain S_P-S_{B_P}-S_{B_O}-S_O; if the system starts from S_P, it must pass S_{B_P} and then S_{B_O} before entering S_O, if any of the sets is nonempty.

Based on this relationship, we show the virtual impedance control in Eq. 14 is stable.

Theorem *Assume that $\ddot{q}_o$ is asymptotically stable when without projection and stable when with projection, and that $\|\ddot{q}_o\| = \mathcal{O}(\|\dot{q}\|^{c_2})$. Let $k_r, b_r > 0$ and $b_r = \mathcal{O}(\|\dot{q}\|^{c_1})$ with $c_1 > \max(1, c_2 - 1)$. If the environment is stationary and $\sup_{r_+ \in [0,\delta]} \partial\phi$ is small enough in respect with σ_{thre} such that the relationship in Eq. 28 holds, the virtual impedance control (14) with $\bar{P}$ and Ψ defined in Eqs. 20 and 21 converges to the set S_{B_O} or S_O in finite time. If it converges in S_{B_O}, the system is bounded; otherwise, the system is asymptotically stable.*

Proof We first consider the case where the system starts from S_O. If it does not pass S_B before the convergence, the system converges asymptotically in S_O; otherwise, it enters S_{B_O}. Next, we consider the case where the system starts fromS_P. Because $\dot{\mathcal{V}}_R = -b_r \|\dot{r}_+\|^2$ in S_P, the system is stable in S_P and goes toward the set $\{q, \dot{q} \in \mathbb{R}^n | \dot{r}_+, r_+ = 0\}$ which is in S_O. However, due to Eq. 28, it must pass S_{B_P}, either on the way or before entering S_O. Starting from S_{B_P}, even with the option to go into S_P, the system eventually goes into the set S_{B_O}, because the dynamics in

the dimensions where $\sigma_i \geq \sigma_{thre}$ follows the projection of Eq. 16. Therefore, to characterize the stability of Eq. 14, it is sufficient to analyze the behavior of the system starting from S_{B_O}.

Suppose the system start from S_{B_O}. For clarity, we consider the scalar case where $k = 1$. Because the basis vectors V, U in singular value decomposition are orthonormal, this result can be generalized to the case where$k > 1$. If $k = 1$ and $q \in S_{B_O}$, the risk space dynamics follows

$$\ddot{r}_+ = \dot{J}\dot{q} + J\ddot{q}_d = -\psi(b_r\dot{r}_+ + k_r r_+) + (1-\psi)(\dot{J}\dot{q} + J\ddot{q}_o). \tag{29}$$

The time-derivative of the Lyapunov candidate (15) becomes

$$\dot{\mathcal{V}}_R = -\psi b_r \|\dot{r}_+\|^2 + (1-\psi)\dot{r}_+^T(\dot{J}\dot{q} + J\ddot{q}_o + k_r r_+), \tag{30}$$

Using Eq. 30, we can characterize the upper-bound of $\mathcal{V}_R$ and $\|\dot{r}_+\|$. Firstly, we show a finite bound exists for the scenario where the system travel along a constant ψ in S_{B_O}. In this case, $\mathcal{V}_R$ is upper-bounded if there exists finite $\|\dot{r}_+\|$such that $\dot{\mathcal{V}}_R$ is negative. Because the indefinite term grows no faster than $O(\|\dot{q}\|^{\max(3,c_2+1)})$ and σ_i is non-zero, $b_r = O(\|\dot{q}\|^{c_1})$ with $c_1 > \max(1, c_2 - 1)$, resulting the negative definite term in Eq. 30 as $O(\|\dot{q}\|^{2+c_1})$, provides a bound for $\mathcal{V}_R$: there is a constant $\dot{r}_{+,\max}$ such that if $\|\dot{r}_+\| > \dot{r}_{+,\max}$, $\dot{\mathcal{V}}_R$ is negative. As a result, $\mathcal{V}_R$ is bounded in S_{B_O}, and so is $\|\dot{r}_+\|$, which converges to

$$\|\dot{r}_+\|^2 \leq \left(\frac{1-\psi}{\psi b_r}\right)^2 \left\|\dot{J}\dot{q} + J\ddot{q}_o + k_r r_+\right\|^2 =: \dot{r}_{+,\max}(\psi). \tag{31}$$

and $\mathcal{V}_R \leq 2^{-1}k_r\|r_+\|^2 + 2^{-1}\left\|\dot{r}_{+,\max}\right\|^2 =: \mathcal{V}_{R,\max}(\psi)$. Note that though $\dot{q}$ appears in the right-hand side of Eq. 31, $\dot{r}_{+,\max}$ is finite for the argument above. Because ψ is a function of q, by definition (15), the upper-bound $\mathcal{V}_{R,\max}(\psi)$ of $\mathcal{V}_R$ in S_{B_O} is a function of ψ.

Then, we interpolate this bound along ψ, as illustrated in Fig. 3, in which the bound $\dot{r}_{+,\max}(\psi)$ decreases as $\psi \to 1$ due to the multiplier $(1-\psi)/\psi$. In particular, at the extremity, $\dot{r}_{+,\max}(1) = 0$ and $\mathcal{V}_{R,\max}(1) = 2^{-1}k_r\|r_+\|^2$. Therefore, $\dot{r}_{+,\max}(\psi)$ and $\mathcal{V}_{R,\max}(\psi)$ characterize the invariant set of the system if the system converges in S_{B_O}.

Finally, we use $\mathcal{V}_{R,\max}(\psi)$ to show that the system converge either in S_{B_O} or S_O. Because of Eq. 28, a system starting from S_{B_O} goes either into S_O or S_P (in the scalar case S_{B_P} is empty; for the vector case, this phenomenon occurs independently in each dimension determined by V). Suppose it starts to go to S_P with $\mathcal{V}_R(t_0)$ at t_0 and returns to S_{B_O} with $\mathcal{V}_R(t_1)$ at t_1. Then $\mathcal{V}_R(t_1) < \mathcal{V}_R(t_0)$. If it does not enter S_O, eventually the sequence $\mathcal{V}_R(t_i)$ converges under $\mathcal{V}_{R,\max}(\psi)$ and

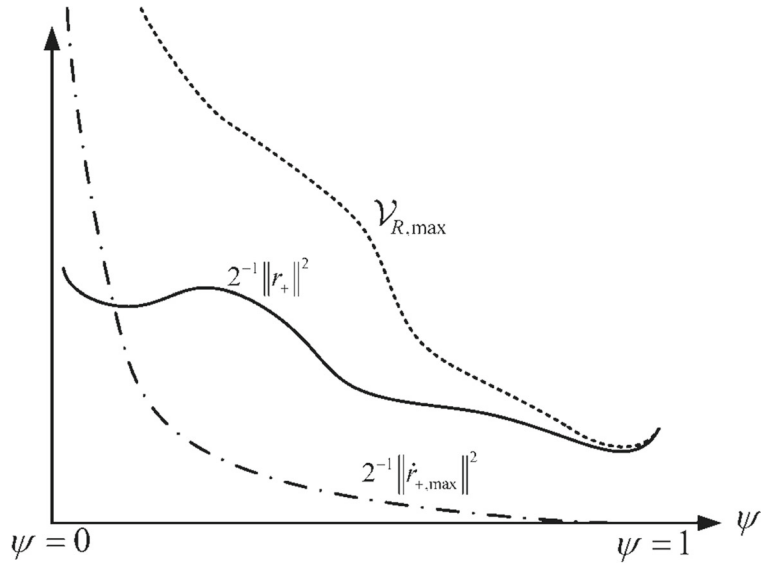

Fig. 3 The upper bound of the Lyapunov candidate V_R

the system stays in S_{B_O} without entering S_P again, because $\mathcal{V}_{R,\max}(1) = 2^{-1}k_r \|r_+\|^2$ and $\dot{r}_{+,\max}(1) = 0$. Otherwise, it leaves S_{B_O} and enters S_O. In this case, the system either converges in S_O if collision avoidance does not further activate, or converges into S_{B_O} due to the previous reasons. Thus, because $\dot{r}_{+,\max}(\psi)$ is bounded and the original dynamics is asymptotically stable S_O, the rest of the theorem follows. □

The bound in the analysis above is conservative, as it does not use the information of $\ddot{q}_o$. Actually, the condition in the boundary layer can also be analyzed in perspective of $\ddot{q}_o$. If $\ddot{q}_o$ is passive, a tighter bound can be obtained. Nevertheless, Theorem shows that if $b_r = O(\|\dot{q}\|^{c_1})$ is with $c_1 > \max(1, c_2 - 1)$, the system achieves the desired behavior: it exhibits consistent dynamics in S_P, follows the original dynamics $\ddot{q}_o$ if possible, and allows $\ddot{q}_o$ to interfere in S_{B_O} so $\ddot{q}_o$ can voluntarily deactivate the collision avoidance without trapping.

The following corollary accompanying the proof of Theorem shows that the discrete-time acceleration-based inverse kinematic control could be intrinsically unstable for large $\dot{q}$ if the damping is constant.

Corollary *Let Δt be the sampling time and $J_x = \partial x/\partial q$ be the Jacobian matrix. The discrete-time acceleration-based inverse kinematic control $\ddot{q}(t) = \ddot{q}_x(s\Delta t)$ for $t \in [s\Delta t, (s+1)\Delta t)$ with constant B_x is unstable if $\|\dot{q}\| \geq \dot{q}_{\max}$, in which*

$$\ddot{q}_x = J_x^{-1}(\ddot{x}_r - K_x\tilde{x} - B_x\dot{\tilde{x}} - \dot{J}\dot{q}), \tag{32}$$

$\dot{q}_{\max}$ is a constant proportional to $\|\partial J_x/\partial q\|$, B_x^{-1}, and Δt^{-1}, $\tilde{x} = x - x_r$, and x_r is the reference trajectory.

Proof The continuous-time control law (32) is designed to realize the second-order dynamics $\ddot{\tilde{x}} + B_x\dot{\tilde{x}} + K_x\tilde{x} = 0$, which is stable in respect to the Lyapunov candidate $\mathcal{V}_X = 2^{-1}\tilde{x}^T K\tilde{x} + 2^{-1}\dot{\tilde{x}}^T\dot{\tilde{x}}$. For the discrete-time version, $\ddot{q}(t) = \ddot{q}_x(s\Delta t)$ for $t \in [s\Delta t, (s+1)\Delta t)$ the time derivative of $\mathcal{V}_X$ becomes $\dot{\mathcal{V}}_X(t) = -\dot{\tilde{x}}^T B_x\dot{\tilde{x}} + \dot{\tilde{x}}^T e$, where $e = \ddot{q}_x(s\Delta t) - \ddot{q}_x(t)$. Because $e = \mathcal{O}(\|\dot{q}\|^2)$, $\dot{\mathcal{V}}_X$ is a polynomial of $\|\dot{q}\|$ of degree three. Therefore, for constant B_x, there is a constant $\dot{q}_{\max}$ which is proportional to $\|\partial J_x/\partial q\|$, B_x^{-1}, and Δt^{-1} such that if $\|\dot{q}\| > \dot{q}_{\max}$, $\dot{\mathcal{V}}_X$ is positive. Since $\mathcal{V}_X$ can be viewed as norm of the system's states, the system is unstable. □

Although Corollary is based on acceleration-based control, the same result applies to torque-based schemes (e.g. Cartesian-space impedance control), as long as $\dot{J}\dot{q}$ is used. On the other hand, if only the first-order derivative is fed back as in velocity-based control, such phenomenon does not happen. We note this unstable phenomenon is independent of the singularity of J_x but due to the inexact cancelation of $\dot{J}\dot{q}$. A similar condition appears in proving the stability of continuous-time control with damped pseudo-inverse in acceleration level [32]. Though in [32]. the stability condition was shown, it only holds for small $\|\dot{q}\|$. Therefore, we posit that the continuous-time acceleration-based control with damped pseudo-inverse is also unstable for large $\|\dot{q}\|$ if the damping varies in different singular directions.

Assume $c_2 \leq 2$. In implementation, we define a variable factor

$$b_f = \begin{cases} (\|\dot{q}\|/\dot{q}_{\max})^2, & \text{if } \|\dot{q}\| \geq \dot{q}_{thre} \\ 1, & \text{else} \end{cases} \tag{33}$$

such that $b_r = b_f b_{r,desired}$, where $b_{r,desired}$ is the desired damping and $\dot{q}_{thre} > 0$ is the threshold. In this paper, we choose $\dot{q}_{thre}$ empirically by simulation. Though $b_f b_{r,desired}$ with arbitrary $\dot{q}_{thre}$ satisfies the stability condition, if $\dot{q}_{thre} > \dot{q}_{\max}$, in which $\dot{q}_{\max}$ is defined with respect to $b_{r,desired}$, there will be an open interval in$\|\dot{q}\|$ such that the chosen derivative of the Lyapunov candidate $\mathcal{V}_R$ is indeterminate; once the system enters the interval, despite stable, $\mathcal{V}_R$ may remain large, which is undesirable. Therefore, in practice, it should be chosen that $\dot{q}_{thre} < \dot{q}_{\max}$.

We neglect the discussion of dynamic environments, so the system can be viewed as an autonomous system parameterized in the joint phase space. For dynamic environment, the characterization of Eq. 25 would depend also on the environment. Due to the requirement on bounded joint acceleration, we can easily see that when the robot is nearly kinematic singular with respect to the upcoming collision, the success of avoidance is determined by the speed and acceleration of the obstacle. On the other hand, when environment's variation is within the capability of the

robot, the property of the proposed systems remains if the information of the obstacle's velocity and acceleration is included in $\dot{r}_+$ and $\ddot{r}_+$. Otherwise, since the overall system is continuous, the system is at least input-to-state stable with regard to the change of environment.

In addition, the Jacobian J in Eq. 6 implicitly assumes the closest point remains the same in respect to the frame on the link. In fact, this point moves during the avoidance. But because the model (1) is continuous, we can expect that the system remains the same stability condition of Theorem by selecting b_r large enough and Δt small enough. Finally, because of time delay due to the discrete-time implementation, the system could oscillate between S_{B_O} and a small portion in $S_{B_P} \cup S_P$, though we did not observe this phenomenon in our simulations and experiments.

4 Simulations and Experiments

4.1 Setup

We demonstrate two simulations and two experiments to exemplify the virtual impedance control with the 6-DOF NTU Robot Arm (NTU Robotics Laboratory). All simulations and experiments were conducted on a PC with CPU Intel Core i5-2500 3.3GHz and 4GB of RAM. The implementation ran on the four-core CPU: one processor executed the proposed risk avoidance control, and the others handled I/O tasks such as motor trajectory transmission, GUI, and the processing of Kinect™ sensor. The geometry of both robot and humans were modelled as collections of spherically extended line segments. For the parameters in the virtual impedance control, $\phi(r) = 3^{-1}r^3$, $\dot{q}_{thre} = 10$ (rad/s), and k_r, b_r are chosen to realize a critically damped system with bandwidth 100 Hz. In this setting, with the environment updated by Kinect™ sensor (30 Hz), our control approach operated in a cycle of 0.05 ms (20 kHz) and sent position command (derived by numerical integration) to the position controller (MCDC 3006s, FAULHABER Inc.) via RS-232 communication port every 5 ms (200 Hz).

4.2 Simulations

In Simulation 1, we test the consistency of the dynamics in the risk space regarding different configurations and discuss the effect of the boundary layer. We initialized the robot with two different poses (zero initial velocity) such that the initial value of the risk functions were similar (0.0466559 and 0.0466565 respectively, as shown in Fig. 4). The original controller was a joint space impedance controller whose goal is to maintain the robot to the initial condition. To better illustrate the behavior, we demonstrated the scenario where the activated risk function was one-dimension to prevent the collision with a ball obstacle in Cartesian space. In this case, the proposed scheme was equivalent to the Cartesian space impedance control in the one-dimensional subspace along the shortest distance to the obstacle. Firstly, we observe that the risk dynamics of the two cases in Fig. 5 are the same regardless of the pose of the robot in S_P (i.e. $\psi(\sigma) = 1$), which is never the case if the collision avoidance scheme is realized by the Jacobian transpose. Inside the boundary layer $\psi(\sigma) < 1$, the original dynamics and the collision avoidance balances; the two simulations converge to slightly different conditions, because the initial poses of the two tests were different. Next,

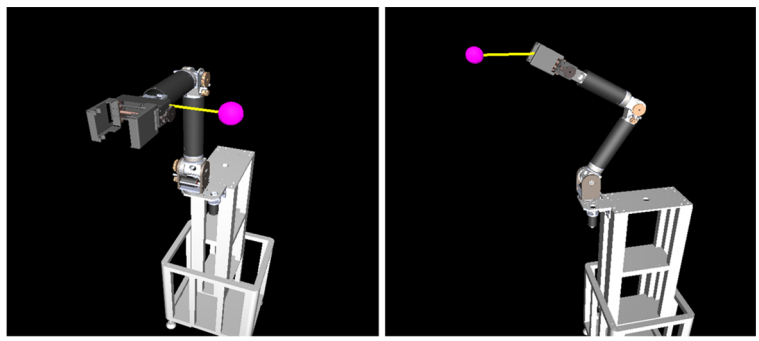

Fig. 4 The initial conditions in Simulation 1

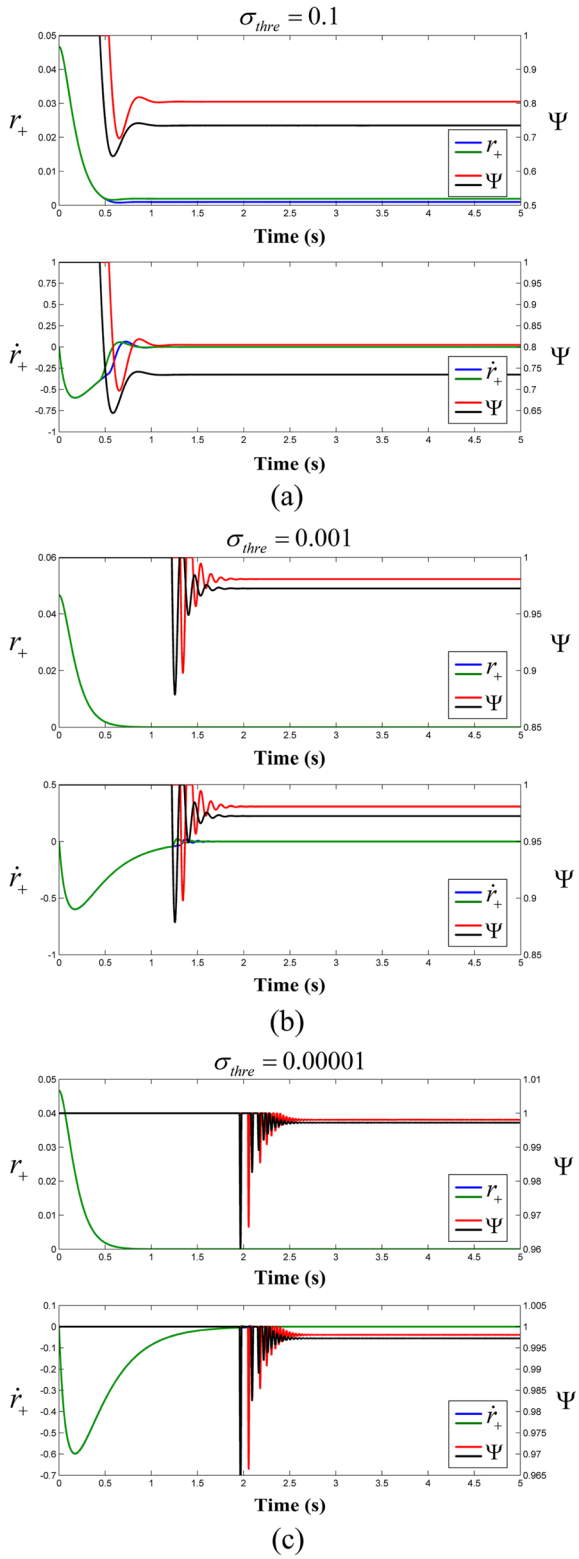

Fig. 5 The consistent risk space dynamics with the boundary layers of different sizes

we compare the responses with boundary layers of different σ_{thre}. The size of the risk function at the equilibrium point is related to the size of the boundary. If the thickness of the boundary layer is large as in the Fig. 5a, the risk function converges to a larger value. Similarly, we can observe that the dynamics of the risk space is consistent only outside the boundary ($\psi(\sigma) = 1$) so overshoot may happen in the boundary layer despite the critically damped risk dynamics. In addition, we can observe the asymptotical behavior of the risk dynamics inside the boundary layer also depends on σ_{thre}. If the boundary layer is large enough as with $\sigma_{thre} = 10^{-1}$, we observe that once the robot enters S_{B_O} it never returns S_P. On the contrary, for $\sigma_{thre} = 10^{-3}$ and $\sigma_{thre} = 10^{-5}$, the robot travels between S_{B_O} and S_P multiple times before finally converging in S_{B_O}. However, the chattering would occur if the thickness is below some threshold as with $\sigma_{thre} = 10^{-5}$. The robot oscillates in the boundary as it is pushed in and out by the original dynamics and by the repulsive force of the obstacle avoidance.

In Simulation 2, we simulate the robot to operate in the condition in the vicinity of singularity and show the change of $\|r_+\|$. The robot's original dynamics was regulated by Cartesian space impedance control. Figure 6a shows the results of the robot operating in the region where J_r was nearly singular (the singular value in the blue line denotes that of the Jacobian of kinematics J_r). In this simulation, an obstacle was placed near the end-effector such that the robot started with a configuration in which J_r is nearly singular yet J_ϕ is stable (i.e. $\|r_+\|$ is large); the original dynamics was to lead the end-effector to the obstacle in order to maintain the initial configuration. As shown in the left gray region, the system started in the boundary layer S_{B_O} because $J = J_\phi J_r$, and the original dynamics presented to increase the risk level. However, due to the small singular value of J_r, as seen in the blue line, the increase of the risk function was negligible. Once it passed S_{B_O} and entered S_P, it escaped the singularity region of J_r and went toward S_{B_O}, where $\|r_+\|$ is small. The rest followed Theorem: it oscillated between S_{B_O} and S_P, but converged to S_{B_O} in finite time. On the other hand, Fig. 6b shows the scenario where the robot operated near the boundary of the collision avoidance scheme where r_+ was close to zero, and the original task was to put the robot close to the obstacle (the singular value in the blue

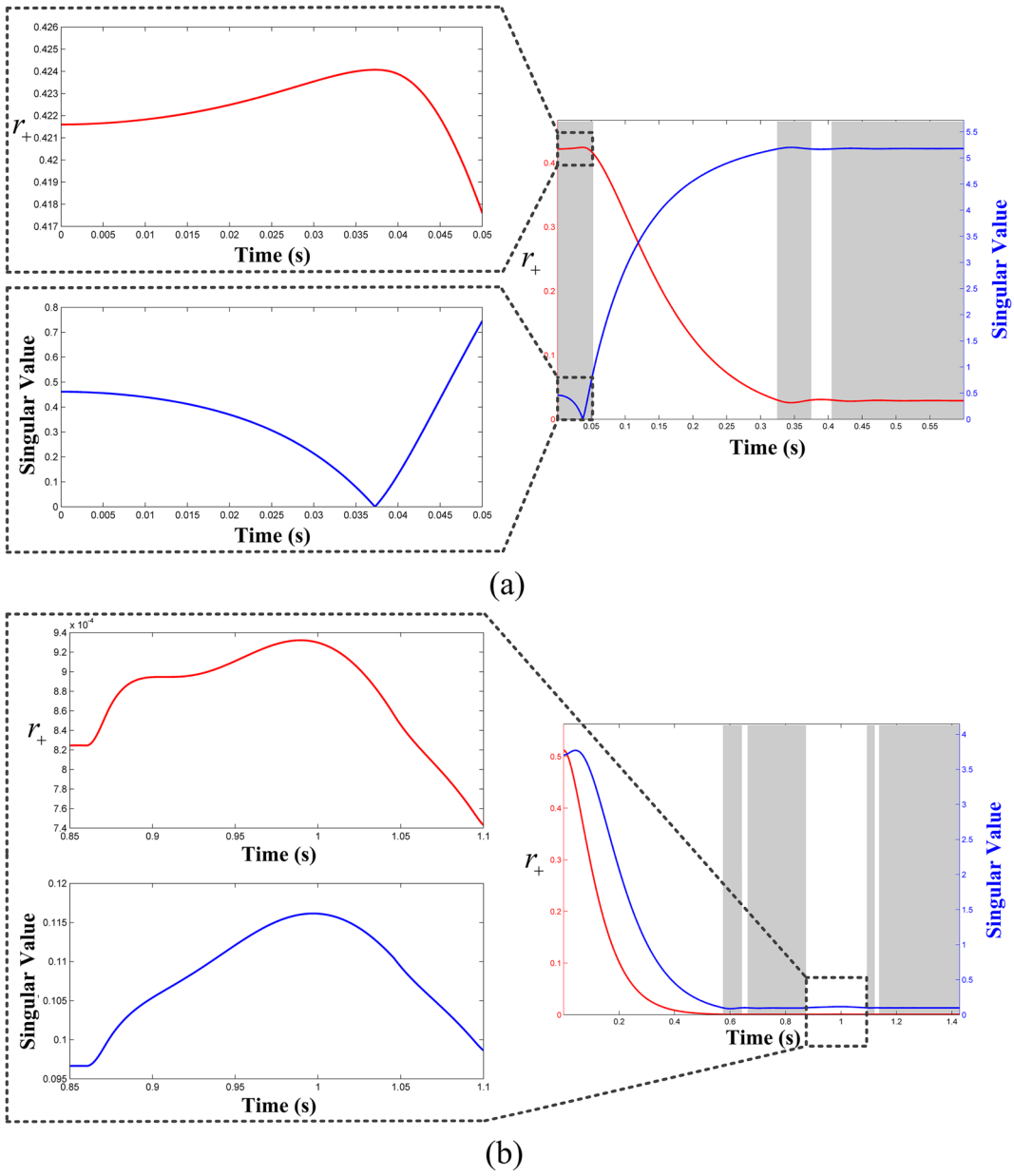

Fig. 6 The robot operates in the condition at the vicinity of singularity of J_r and $J_\emptyset$ respectively. The blue line denotes singular value. The red line denotes $\|r_+\|$. The light gray area denotes operating in the boundary layer. **a** The robot operates in the region where J_r is close singular. **b** The robot operates in the boundary of the collision avoidance scheme (i.e. r_+ is close to zero)

line denotes that of the Jacobian of risk function J_ϕ). As previously, the system entered S_{B_O} from S_P, and converged in finite time despite oscillation. Therefore, the problem of kinematic singularity and activation of collision avoidance are resolved in the boundary layer.

In Simulation 3, the proposed virtual impedance control is compared with two other conventional control methods: the transpose-Jacobian approach,

$$\ddot{q}_{TJ} = J^T(-k_r r_+ - b_r \dot{r}_+) + (I - J^+ J) \times J_x^T(-K_x(x - x_r) - B_x(\dot{x} - \dot{x}_r)) \quad (34)$$

and the velocity-level approach [13],

$$\dot{q}_{VL} = \lambda J^{\dagger}\upsilon_0 + (I - \lambda J^{\dagger}J) \times J_x^{\dagger}(-K_x(x - x_r)), \tag{35}$$

where υ_0 is a scalar representing the nominal avoiding velocity ($\upsilon_0 = 1$), $\lambda(\|d_{closest}\|)$ is defined as

$$\lambda(\|d_{closest}\|) = \begin{cases} \left(\frac{d_m}{\|d_{closest}\|}\right)^n, & \|d_{closest}\| \geq d_m \\ 1, & \|d_{closest}\| < d_m \end{cases} \tag{36}$$

Note that $d_{closest}$ is the vector connecting the closest points between the obstacle and the robot, d_m is the critical distance [13] to the obstacle ($d_m = 15$ (cm)), n is positive number ($n = 7$). In attempt to compare different approaches, we chose $\bar{d}_{C,i} = 34.67$ (cm) in our proposed approach such that $\lambda(\bar{d}_i) = 0.15$, which we treated as the activation of Eq. 35; all approaches were set with $K_x = 10$ and $B_x = 6.3246$ (critically damped).

We consider the case where a single obstacle is placed near the end-effector of the robot (similar to Simulation 1). The three approaches were initialized with the same initial condition. The primary task was obstacle avoidance and the secondary task was position tracking of the end-effector. Figure 7 shows the comparison results in terms of the closest distance between the robot and the obstacle, the change of $\|r_+\|$, and the tracking error $\|x_r - x\|$. As shown in the top and the middle plots, the proposed approach responds quickly and smoothly to keep the safe distance, with a lower risk of collision than Eqs. 34 and

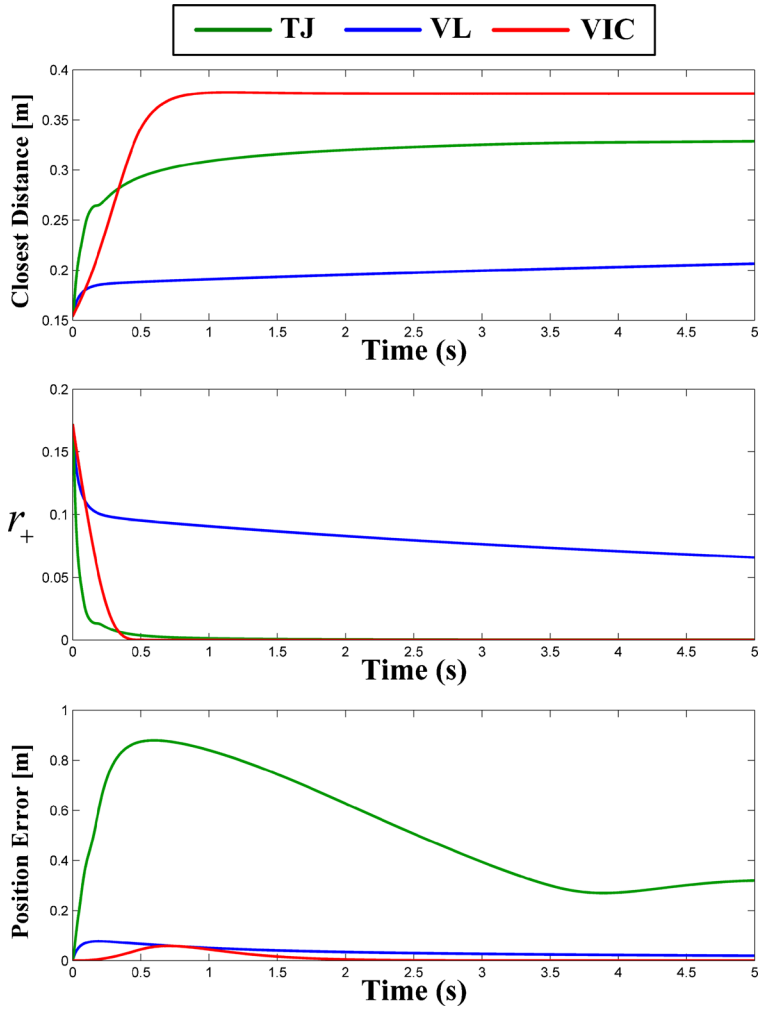

Fig. 7 Comparison of obstacle avoidance with the transpose-Jacobian controller (TJ) (34), the velocity-level controller (VL) (35), and the proposed controller (VIC). The top plot shows the result of the closest distance between the robot and the obstacle. The middle plot shows the risk value and the bottom plot shows the tracking error of the end-effector

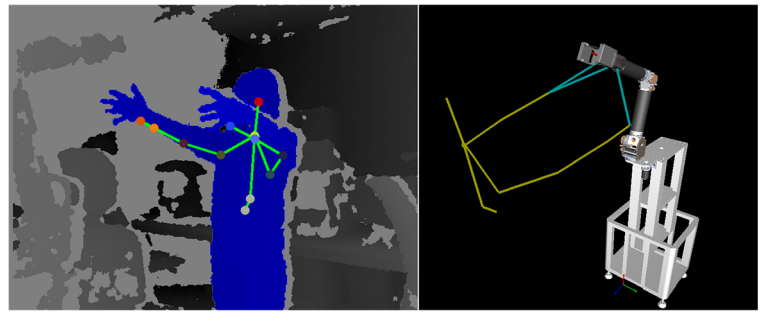

Fig. 8 The modeling of the human and the robot

35. The bottom plot shows the end-effector's tracking error. We can see that, when using Eq. 34, the tracking error is more significant than Eq. 35 and the proposed approach during avoiding the obstacle. This means that the interference occurred between different priorities. From this comparison between different obstacle avoidance controllers, we observe that the proposed controller presents smooth transitions

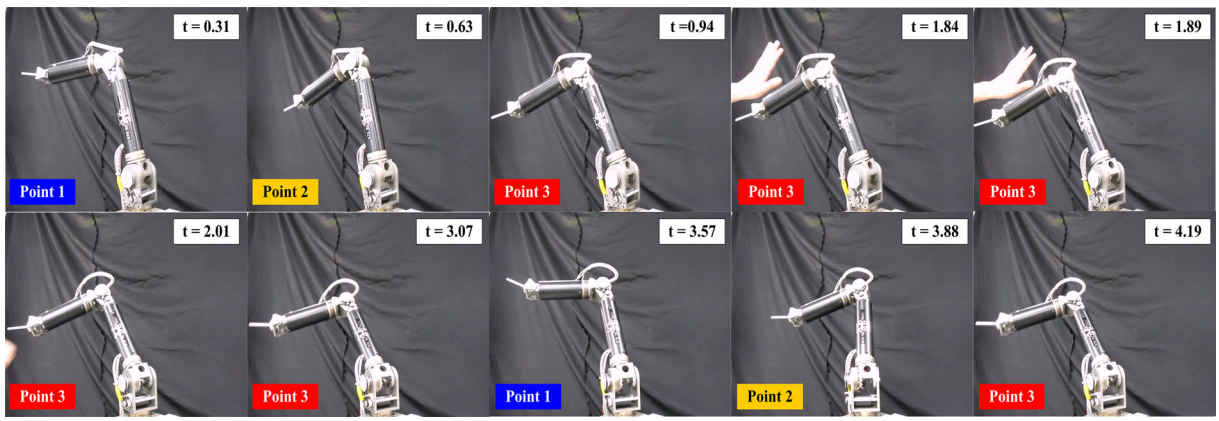

(a)

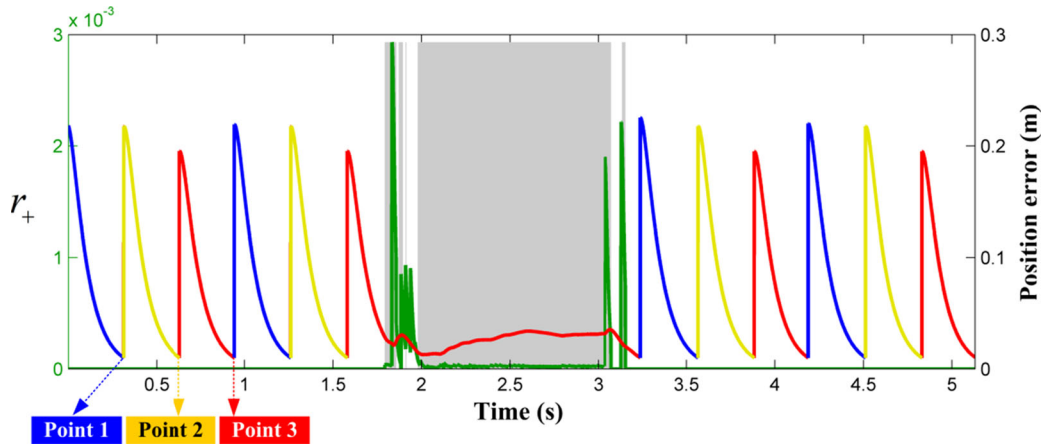

(b)

Fig. 9 The results of Experiment 1 **a** The snapshots of the experiment **b** The changes of the position error and $\|r_+\|$ during the task transition. The blue line denotes $\|r_+\|$. The red line denotes position error. The light gray area denotes the operations in the boundary layer

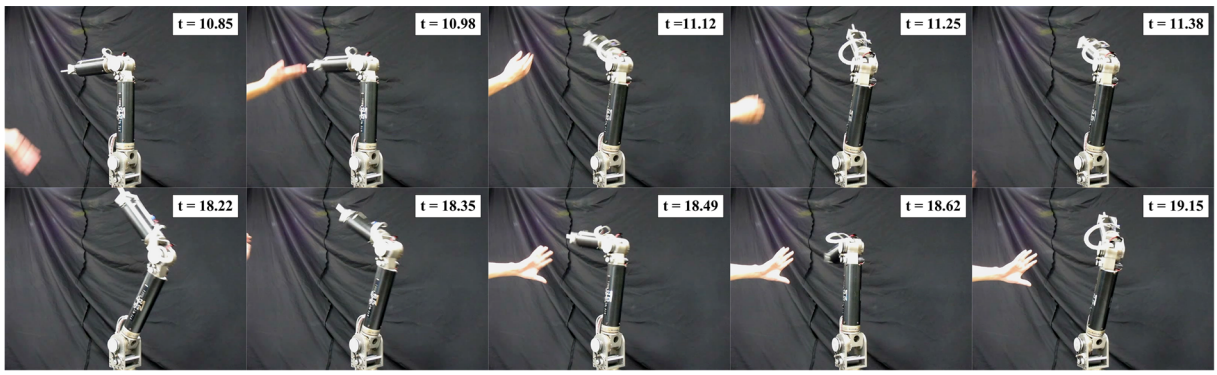

Fig. 10 The snapshots of Experiment 2, in which the human attempted to touch the robot

between tasks of different priorities and performs immediate evasive maneuvers.

4.3 Experiments

In the experiments, the original task of the robot was to continuously follow a predefined movement. The workspace of the robot was kept under surveillance by the Kinect™ sensor to detect human skeletons. With the SDK of Kinect™, the skeleton of the human can be identified in the depth image and then incorporated into our proposed risk avoidance control scheme. In Fig. 8, the light blue lines represent the direction to the upcoming collisions and the other line segments denote models of the robot and the human. The parameters of the proposed approach was selected as $\bar{d}_{C,i} = 25$ (cm), $\bar{d}_{J,i} = 10$ (degrees), $k_r = 100$, $b_r = 20$, and $\sigma_{thre} = 0.01$.

In Experiment 1, using position Cartesian space impedance control, the robot was tracking a triangular position trajectory in Cartesian space (the space of orientation was controlled by a pure damping control for numerical stability, which was turned off once the collision avoidance activated). The snapshots are shown in Fig. 9a (please refer to the accompanying video **exp1.avi**); Fig. 9b shows the changes of the position error and $\|r_+\|$ during task transition. When the obstacle appeared near the motion trajectory of the robot elbow at t =1.79s, the robot tried to exploit its task redundancy to continue to execute the desired end-effector trajectory while avoiding the obstacle. We can see that the original Cartesian trajectory tracking task operated in the subspace of the active Jacobian matrix J when the collision avoidance turned on. However, when the subspace was not large enough (i.e. task redundancy was insufficient), the robot motion was dominated by the collision avoidance (from t =1.79–3.16 (s)). After the constraint was released, the robot then regained sufficient redundancy in the null space of the collision avoidance task to continue the position tracking control of the end-effector (from t =3.16 (s) to t =5.13 (s)). As shown, the proposed collision avoidance control scheme can exploit the remaining redundancy to complete the original task, and can smoothly transit between the activation and the deactivation of the collision avoidance.

The scenario in Experiment 2 is related to the issue of human-robot coexistence. In this experiment, the human attempted to touch the robot while the robot was performing an immediate evasive maneuver with the proposed risk avoidance control scheme. Figure 10 shows the snapshots of the experiment (please refer to the accompanying video **exp2.avi**). With the proposed control scheme, the robot followed the direction of the human and did not come any closer than the safe zone indicated by $\bar{d}_i$. We can observe that the motion of the robot was smooth due to the controlled impedance. Consequently, regardless of the type of collision, the robot presents satisfactory and consistent performance that is both physically and perceptionally safe.

5 Conclusions

For safe human-robot interaction, we propose virtual impedance control which regulates the dynamics of collision avoidance as a second-order linear response in an abstract vector space, the risk space. We treat the safety problem as a multi-priority problem,

ensuring avoidance-first concept and operating the original dynamics in the null space. By the boundary layer defined on the spectral of the Jacobian matrix, we show that the proposed scheme can stably transit between normal operation and collision avoidance with continuous acceleration, providing that the original dynamics is stable with or without projection matrix. As a consequence, the robot can avoid any collision smoothly and consistently regardless of the types of potential collisions. In the experiments, we integrated the 6-DOF NTU Robot Arm with Kinect™ to detect dynamic environment to demonstrate our approach for safe robot operation with human nearby. In our future studies, we want to incorporate physical forces into the risk space. While the risk space dynamics now consists of only an initial response, a forcing term can be defined by a map to transfer the physical contact force into the system. Handling physical interactions undetectable by computer vision, this approach could improve the system's performance and is suitable for close collaborative scenarios, in which the robot could contact with humans up to certain safety measure.

Compliance with Ethical Standards The authors declare that they have no conflict of interest.

References

1. Pedrocchi, N., Vicentini, F., Matteo, M., Tosatti, L.M.: Safe human-robot cooperation in an industrial environment. Int. J. Adv. Robot. Syst. **10**(26) (2013)
2. Shi, J., Jimmerson, G., Pearson, T., Menassa, R.: Levels of human and robot collaboration for automotive manufacturing. In: Workshop Perform. Metr. Intell. Syst., Maryland, pp. 95–100 (2012)
3. Matthias, B., Kock, S., Jerregard, H., Kallman, M., Lundberg, I., Mellander, R.: Safety of collaborative industrial robots: certification possibilities for a collaborative assembly robot concept (2011)
4. Heyer, C.: Human-robot interaction and future industrial robotics applications. In: IEEE/RSJ Int. Conf. Intell. Robot. Syst., Taipei, pp. 4749–4754 (2010)
5. Haddadin, S., Parusel, S., Belder, R., Albu-Schaffer, A., Hirzinger, G.: Safe acting and manipulation in human environments: a key concept for robots in our society. In: IEEE Workshop Adv. Robot. Its Soc. Impacts, Half-Moon Bay, pp. 72–75 (2011)
6. Lasota, P.A., Rossano, G.F., Shah, J.A.: Toward safe close-proximity human-robot interaction with standard industrial robots. In: IEEE Int. Conf. Autom. Sci. Eng., Taipei, pp. 339–344 (2014)
7. Mitka, E., Gasteratos, A., Kyriakoulis, N., Mouroutsos, S.G.: Safety certification requirements for domestic robots. Saf. Sci. **50**(8), 1888–1897 (2012)
8. Vasic, M., Billard, A.: Safety issues in human-robot interactions. In: IEEE Int. Conf. Robot. Autom., Karlsruhe, Germany, pp. 197-204 (2013)
9. Sentis, L., Park, J., Khatib, O.: Compliant control of multicontact and center-of-mass behaviors in humanoid robots. IEEE Tran. Robot. **26**(3), 483–501 (2010)
10. Taïx, M., Flavigné, D., Ferré, E.: Human interaction with motion planning algorithm. J. Intell. Robot. Syst. **67**(3–4), 285–306 (2012)
11. Arkin, R.C.: Integrating behavioral, perceptual, and world knowledge in reactive navigation. J. Robot. Auton. Syst. **6**(1), 105–122 (1990)
12. Dietrich, A., Wimbock, T., Albu-Schaffer, A., Hirzinger, G.: Integration of reactive, torque-based self-collision avoidance into a task hierarchy. IEEE Tran. Robot. **28**(5), 1278–1293 (2012)
13. Petrič, T., Lajpah, L.: Smooth continuous transition between tasks on a kinematic control level: obstacle avoidance as a control problem. J. Robot. Auton. Syst. **61**(8), 948–959 (2013)
14. Dietrich, A., Wimbock, T., Taubig, H., Albu-Schaffer, A., Hirzinger, G.: Extensions to reactive self-collision avoidance for torque and position controlled humanoids. In: IEEE Int. Conf. Robot. Autom., Shanghai, pp. 3455–3462 (2011)
15. Flacco, F., Kroeger, T., De Luca, A., Khatib, O.: A Depth Space Approach for Evaluating Distance to Objects. J. Intell. Robot. Syst., 1–16 (2014)
16. Stasse, O., Escande, A., Mansard, N., Miossec, S., Evrard, P., Kheddar, A.: Real-time (self)-collision avoidance task on a hrp-2 humanoid robot. In: IEEE Int. Conf. Robot. Autom. Pasadena, pp. 3200–3205 (2008)
17. Khatib, O.: Real-time obstacle avoidance for manipulators and mobile robots. Int. J. Robot. Res. **5**(1), 90–98 (1985)
18. Brock, O., Khatib, O., Viji, S.: Task-consistent obstacle avoidance and motion behavior for mobile manipulation. In: IEEE Int. Conf. Robot. Autom., Washington, pp. 388–393 (2002)
19. Dietrich, A., Wimbock, T., Albu-Schaffer, A.: Dynamic whole-body mobile manipulation with a torque controlled humanoid robot via impedance control laws. In: IEEE/RSJ Int. Conf. Intell. Robot. Syst., San Francisco, pp. 3199–3206 (2011)
20. Flacco, F., Kroger, T., De Luca, A., Khatib, O.: A depth space approach to human-robot collision avoidance. In: IEEE Int. Conf. Robot. Autom., Saint Paul, pp. 338–345 (2012)
21. García-Delgado, L., Noriega, J., Berman-Mendoza, D., Leal-Cruz, A., Vera-Marquina, A., Gómez-Fuentes, R., García-Juárez, A., Rojas-Hernández, A., Zaldívar-Huerta, I.: Repulsive Function in Potential Field Based Control with Algorithm for Safer Avoidance. J. Intell. Robot. Syst., 1–12 (2014)
22. Haddadin, S., Belder, R., Albu-Schäffer, A.: Dynamic motion planning for robots in partially unknown environments. In: IFAC World Congres., Milano, Italy, p. 2011
23. Scott, N.A., Carignan, C.R.: A line-based obstacle avoidance technique for dexterous manipulator operations. In:

IEEE Int. Conf. Robot. Autom., Pasadena, pp. 3353–3358 (2008)
24. Sentis, L., Khatib, O.: A whole-body control framework for humanoids operating in human environments. In: IEEE Int. Conf. Robot. Autom., Orlando, pp. 2641–2648 (2006)
25. Dietrich, A., Wimbock, T., Albu-Schaffer, A., Hirzinger, G.: Reactive whole-body control: Dynamic mobile manipulation using a large number of actuated degrees of freedom. IEEE Robot. Autom. Mag. **19**(2), 20–33 (2012)
26. Haddadin, S., Parusel, S., Belder, R., Vogel, J., Rokahr, T., Albu-Schäffer, A., Hirzinger, G.: Holistic design and analysis for the human-friendly robotic co-worker. In: IEEE/RSJ Int. Conf. Intell. Robot. Syst., Taipei, pp. 4735–4742 (2010)
27. Haddadin, S., Urbanek, H., Parusel, S., Burschka, D., Rossmann, J., Albu-Schaffer, A., Hirzinger, G.: Real-time reactive motion generation based on variable attractor dynamics and shaped velocities. In: IEEE/RSJ Int. Conf. Intell. Robot. Syst. Taipei, pp. 3109–3116 (2010)
28. De Santis, A., Albu-Schäffer, A., Ott, C., Siciliano, B., Hirzinger, G.: The skeleton algorithm for self-collision avoidance of a humanoid manipulator. In: IEEE/ASME Int. Conf. Adv. Intell. Mech., Zurich, pp. 1–6 (2007)
29. Sugiura, H., Gienger, M., Janssen, H., Goerick, C.: Real-time self collision avoidance for humanoids by means of nullspace criteria and task intervals. In: IEEE/RAS Int. Conf. Humanoid Robot., Genova, pp. 575–580 (2006)
30. Khatib, O.: A unified approach for motion and force control of robot manipulators: the operational space formulation. IEEE Tran. Robot. Autom. **3**(1), 43–53 (1987)
31. Chiaverini, S.: Singularity-robust task-priority redundancy resolution for real-time kinematic control of robot manipulators. IEEE Tran. Robot. Autom. **13**(3), 398–410 (1997)
32. Caccavale, F., Chiaverini, S., Siciliano, B.: Second-order kinematic control of robot manipulators with Jacobian damped least-squares inverse: theory and experiments. IEEE/ASME Tran. Mech. **2**(3), 188–194 (1997)

Sheng-Yen Lo received B.S. and M.S. degrees from Chun Yun Christian University, Chungli, Taiwan in 2006 and 2008, respectively. He is currently a Ph.D. student at NTU Robotics Laboratory, Department of Mechanical Engineering, National Taiwan University, Taipei, Taiwan. His current research interests include visual sevoing and safe human robot interaction.

Ching-An Cheng received double B.S. degrees in mechanical engineering and electrical engineering from National Taiwan University, Taipei, Taiwan, in 2011, and M.S. degree in mechanical engineering from National Taiwan University in 2013. Currently, he is pursuing Ph.D. degree in robotics at Georgia Institute of Technology. His research has been concerned with robot control and learning, reproducing kernel Hilbert space, system dynamics and identification, human-robot interaction, and exoskeletons.

Han-Pang Huang received M.S. and Ph.D. degrees in electrical engineering from The University of Michigan, Ann Arbor in 1982 and 1986, respectively. Since 1986 he has been with National Taiwan University, Taipei, Taiwan, where he is currently a distinguished professor and Zhong Zhuo Zhang Chair Professor in the Department of Mechanical Engineering and the Graduate Institute of Industrial Engineering and serves as the Director of NTU Robotics Laboratory. His research interests include intelligent robotic systems, humanoid robots, prosthetic hands, manufacturing automation, machine intelligence, and nonlinear systems.